RESEARCH ARTICLE OPEN ACCESS

Performance of Thermal Radiation Energy on Stagnation-Point Flow In The Presence of Water Based Copper and Single Walled Carbon Nanotubes over Stretching/Shrinking Sheet

[1]R. Kandasamy, [2] R. Dharmalingam, And [3] K.K. Sivagnana Prabhu
[1]Faculty Of Science, Technology And Human Development, Universiti Tun Hussein Onn Malaysia, Malaysia.
[2] Department Of Mechanical Engineering, SNS College Of Technology, Coimbatore, India.
[3]Department Of Chemical Engineering, R.M.K. Engineering College, Anna University, India.

ABSTRACT
This article is expected for analyzing the impact of mixed convection flow of water based copper and single walled carbon nanotubes on a stagnation-point flow over a porous stretching/shrinking sheet subject to thermal energy radiation by utilizing numerical method. The governing PDEs are converted into nonlinear ODEs by using similarity transformation which is solved numerically using fifth-order Runge–Kutta–Fehlberg method with shooting technique (MAPLE 18). Both stretching and shrinking sheets, the influences of governing parameters are analyzed in graphical and tabular form and found that the SWCNTs–water exhibits higher mass transfer rates compared to Cu–water nanofluids with increase of chemical reaction.
Keywords: SWCNTs-water, Cu-water, MHD mixed convection flow, Thermal energy radiation, Chemical reaction.

I. INTRODUCTION

Nanofluids are used to obtain the high thermal properties at the lowest possible concentrations. Choi et al. [1] predicted that the adding nanoparticles to the base fluid doubled the thermal conductivity of the fluid. Nanofluids has a large amount of applications, coolants for nuclear reactors, cancer therapy and safer surgery by cooling, vehicle computers and transformer cooling, Buongiorno and Hu [2], Kim et al. [3] and Zhu et al.[4]. Buongiorno and Hu [5] investigated the role of nanofluids on nuclear reactor applications. Stagnation-point nanofluid flow model plays a dominant role in chemical and manufacturing processes, polymer extrusion, continuous casting of metals, wire drawing and glass blowing, Gorla et al. [6], Uddin et al. [7], Hamad and Ferdows [8], Rana and Bhargava [9] and Rosca et al. [10].

Magnetohydrodynamic (MHD) convective nanofluid flow has considerable interest in electrical technology, geothermal engineering, nuclear fusion energy transformation, MHD power plant systems and metallurgy engineering, Rabikumar et al. [11], Rahman et al. [12], Kandasamy et al. [13] and AbdEl-Gaied and Hamad [14]. Thermal radiation energy consists of the kinetic energy of random movements of nanoparticle in the base fluid. Thermal radiation energy performs a reorganization of thermal energy into electromagnetic energy and it is one of the major mechanisms of thermal conductivity and diffusivity of the nanoparticles in the base fluid. Thermal radiation energy in the presence of a magnetic field is a high strength of electromagnetic radiation generated by the thermal motion of charge nanoparticles in the base fluid. The high thermal conductivity of single walled carbon nanotubes has an extensive potential for significant heat transfer enhancement. Applications of SWCNTs in thermal administration have recently interested powerful engrossment.

Based on the literature survey, the effects of MHD mixed convective stagnation-point nanofluid flow over a porous stretching/shrinking sheet in water based SWCNTs have not been investigated. The aim of this study is to analyze the effects of water based copper and SWCNTs on MHD mixed convective stagnation-point flow over a porous medium. Thermophysical properties of the fluid and nanoparticles are provided in Table 1.

II. MATHEMATICAL ANALYSIS

It is considered that the steady two-dimensional stagnation-point flow of nanofluids over a porous stretching/shrinking sheet with the velocity $u_w = cx$ (stretching sheet) and $u_w = -cx$ (shrinking sheet) having free stream velocity $U(x) = ax$, where a and c are constants. Let x be the coordinate measured along the stretching/shrinking surface and y is the coordinate measured normal to the stretching/shrinking surface, Fig. 1. The wall/ambient temperature and concentration of the nanofluid are considered as T_w, C_w / T_∞, C_∞. The inflexible magnetic strength B_0 is constructed parallel to the y-axis and the induced magnetic field and the electric polarization charges are negligible. The base fluid and the nanoparticles are in thermal equilibrium and there is no slip occurs between them. The basic steady conservation of momentum, thermal and diffusion equations can be written as

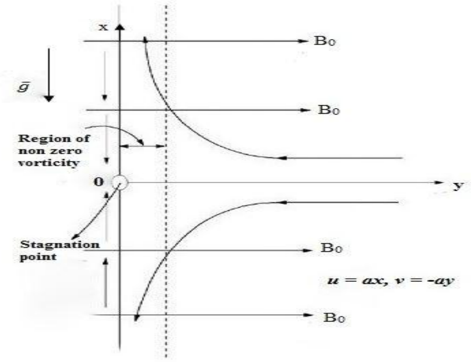

Fig. 1.Physical model and the coordinate system

$$\frac{\partial u}{\partial x}+\frac{\partial v}{\partial y}=0 \tag{1}$$

$$u\frac{\partial u}{\partial x}+v\frac{\partial u}{\partial y}=U\frac{dU}{dx}+\frac{\mu_{nf}}{\rho_{nf}}\frac{\partial^2 u}{\partial y^2}+\left(\frac{\mu_{nf}}{K\,\rho_{nf}}+\frac{\sigma B_0^2}{\rho_{nf}}\right)(U-u)+\frac{(\rho\beta_T)_{nf}}{\rho_{nf}}g(T-T_\infty)+\frac{(\rho\beta_C)_{nf}}{\rho_{nf}}g(C-C_\infty) \tag{2}$$

$$u\frac{\partial T}{\partial x}+v\frac{\partial T}{\partial y}=\alpha_{nf}\frac{\partial^2 T}{\partial y^2}+\frac{Q_0}{(\rho c_p)_{nf}}(T-T_\infty)-\frac{1}{(\rho c_p)_{nf}}\frac{\partial q_r}{\partial y}+\frac{\mu_{nf}}{(\rho c_p)_{nf}}\left(\frac{\partial u}{\partial y}\right)^2 \tag{3}$$

$$u\frac{\partial C}{\partial x}+v\frac{\partial C}{\partial y}=D_{nf}\frac{\partial^2 C}{\partial y^2}-K_1(C-C_\infty) \tag{4}$$

Boundary conditions for stretching and shrinking sheets are

$$u=u_w=\pm cx,\ v=-v_w,\ T=T_w=T_\infty+bx^2,\ C=C_w=C_\infty+bx^2$$
at $y=0$

$$u\to U=ax,\ v\to 0,\ T\to T_w,\ C\to 0 \text{ as } y\to\infty \tag{5}$$

(u, v) - velocity factor along the (x, y) directions, U - stagnation-point velocity in the inviscid free stream, K - permeability of the porous media, g - acceleration due to gravity, Q_0 - heat generation or absorption coefficient, D_{nf} - species diffusivity, K_1 - rate of chemical reaction, a, b, c - positive constants, v_w - the wall mass flux with $v_w > 0$ - suction and $v_w < 0$ - injection, ρ - fluid density, μ_{nf} - coefficient of viscosity of the nanofluid, $(\beta_C)_{nf}$ - concentration expansion of nanofluid, $(\beta_T)_{nf}$ - thermal expansion of nanofluid, K_{nf} - thermal conductivity of the nanofluid, α_{nf} - thermal diffusivity of the nanofluid, ρ_{nf} - effective density of the nanofluid, $(\rho c_p)_{nf}$ - heat capacitance of the nanofluid, which are determined as follows:

$$\rho_{nf}=(1-\varphi)\rho_f+\varphi\rho_s,\ v_{nf}=\frac{\mu_{nf}}{\rho_{nf}},\ D_{nf}=(1-\varphi)D_f$$

$$\alpha_{nf}=\frac{k_{nf}}{(\rho c_p)_{nf}},$$

$$(\rho\beta_C)_{nf}=(1-\varphi)(\rho\beta_C)_f+\varphi(\rho\beta_C)_s,$$

$$(\rho c_p)_{nf}=(1-\varphi)(\rho c_p)_f+\varphi(\rho c_p)_s,$$

$$\frac{k_{nf}}{k_f}=\left\{\frac{(k_s+2k_f)-2\varphi(k_f-k_s)}{(k_s+2k_f)+2\varphi(k_f-k_s)}\right\},$$

$$(\rho\beta_T)_{nf}=(1-\varphi)(\rho\beta_T)_f+\varphi(\rho\beta_T)_s \tag{6}$$

μ_f - viscosity of base fluid, k_f and k_s - thermal conductivities of the base fluid and nanoparticles while ρ_f and ρ_s - density of the base fluid and nanoparticles.

Applying Rosseland approximation $q''_{rad}=q_r=-\frac{4\sigma_1}{3k^*}\frac{\partial T^4}{\partial y}$ (Dulal and Gopinath Mandal [15]), σ_1 - Stefan–Boltzmann constant, k^* - mean absorption coefficient. By Taylor's series expansion of T^4 being $T^4\cong 4T_\infty^3 T-3T_\infty^4$.

$$\frac{\partial q_r}{\partial y}=-\frac{16\sigma_1 T_\infty^3}{3k^*}\frac{\partial^2 T}{\partial y^2} \tag{7}$$

Similarity transformation with stream functions, Dulal and Gopinath Mandal [15] are defined as

$$\eta=\sqrt{\frac{c}{v_f}}\,y,\ \psi=\sqrt{c\,v_f}\,x\,f(\eta),$$

$$\theta=\frac{T-T_\infty}{T_w-T_\infty},\ \varphi=\frac{C-C_\infty}{C_w-C_\infty},\ u=\frac{\partial\psi}{\partial y},\ v=-\frac{\partial\psi}{\partial x}$$

Equations (2-4) with boundary conditions become

$$f'''+\varphi_1\left(\frac{a^2}{c^2}-(f')^2+f\,f''\right)+(\lambda+M\varphi_5)\left(\frac{a}{c}-f'\right)+\varphi_4\gamma_1(\theta+\gamma\,\varphi)=0 \tag{9}$$

$$\frac{1}{\Pr}\left(\frac{K_{nf}}{K_f}+N_r\right)\theta''+\delta\theta+\frac{Ec}{\varphi_5}\left(f''\right)^2+\varphi_6 f\theta'-2\varphi_6 f'\theta=0 \qquad (10)$$

$$\varphi''+\frac{Sc}{\varphi_7}\left(f\varphi'-2f'\varphi-\gamma_2\varphi\right)=0$$

$$\varphi_1=(1-\varphi+\varphi\frac{\rho_s}{\rho_f})(1-\varphi)^{2.5},$$

$$\varphi_2=(1-\varphi+\varphi\frac{(\rho\beta_T)_s}{(\rho\beta_T)_f}),$$

$$\varphi_3=(1-\varphi+\varphi\frac{(\rho\beta_C)_s}{(\rho\beta_C)_f})$$

$$\varphi_4=(1-\varphi+\varphi\frac{(\rho\beta_T)_s}{(\rho\beta_T)_f})\,(1-\varphi)^{2.5},$$

$$\varphi_5=(1-\varphi)^{2.5},\varphi_6=\{1-\varphi+\varphi\frac{(\rho c_p)_s}{(\rho c_p)_f}\},$$

$$\varphi_7=(1-\varphi) \qquad (12)$$

Boundary conditions are

$$f(0)=S,\ f'(0)=\pm 1,\theta(0)=1,\varphi(0)=1,\ f'(\infty)=\frac{a}{c},\theta(\infty)=0, \qquad (13)$$

$\Pr=\frac{\nu_f}{\alpha_f}$ - Prandtl number, $Sc=\frac{\nu_f}{D_f}$ - Schmidt number, $Ec=\frac{u_w^2}{\Delta T(c_p)_f}$ - Eckert number, $M=\frac{\sigma B_0^2 x}{u_w\rho_f}$ - Magnetic parameter, $Nr=\frac{4\sigma_1\theta_w^3}{k_f k^*}$ - Thermal energy radiation parameter, $\gamma=\frac{(\beta_C)_f\Delta C}{(\beta_T)_f\Delta T}$ - Buoyancy ratio, $\gamma_1=\frac{(\beta_T)_f g\Delta Tx}{u_w^2}$ - Mixed convection parameter, $\gamma_2=\frac{K_1 x}{u_w}$ - Chemical reaction parameter, $\delta=\frac{Q_0 x}{(\rho c_p)_f u_w}$ - Heat source / sink parameter and $\lambda=\frac{\nu_f x}{K u_w}$ - Porous parameter. The skin friction coefficient, Nusselt and Sherwood numbers are defined as

$$C_f=\frac{\mu_{nf}}{\rho_f u_w^2}\left(\frac{\partial u}{\partial y}\right)_{at\ y=0}=-\frac{1}{(1-\zeta)^{2.5}}\left(\mathrm{Re}\ x\right)^{-\frac{1}{2}}f''(0)$$

$$Nu_x=\frac{\left\{xK_{nf}\left(-\frac{\partial T}{\partial y}\right)-\frac{4\sigma_1}{3k^*}\left(-\frac{\partial T^4}{\partial y}\right)\right\}_{at\ y=0}}{K_f(T_w-T_\infty)}=-\frac{K_{nf}}{K_f}\left(1+Nr\right)\left(\mathrm{Re}\ x\right)^{\frac{1}{2}}\theta'(0) \qquad (11)$$

and

$$Sh_x=-\frac{x}{(C_w-C_\infty)}\left(\frac{\partial C}{\partial y}\right)_{at\ y=0}=-\left(\mathrm{Re}\ x\right)^{\frac{1}{2}}\varphi'(0)$$

$\mathrm{Re}\ x=\frac{U\ x}{\nu_f}$ - Local Reynolds number.

III.NUMERICAL SOLUTION

Equations (9) and (11) with the boundary condition (13) are reduced into the system of first order ordinary differential equations as

$$\varphi_1=(1-\varphi+\varphi\frac{\rho_s}{\rho_f})(1-\varphi)^{2.5},$$

$$\varphi_2=(1-\varphi+\varphi\frac{(\rho\beta_T)_s}{(\rho\beta_T)_f}),$$

$$\varphi_3=(1-\varphi+\varphi\frac{(\rho\beta_C)_s}{(\rho\beta_C)_f})$$

$$\varphi_4=(1-\varphi+\varphi\frac{(\rho\beta_T)_s}{(\rho\beta_T)_f})\,(1-\varphi)^{2.5},$$

$$\varphi_5=(1-\varphi)^{2.5},\varphi_6=\{1-\varphi+\varphi\frac{(\rho c_p)_s}{(\rho c_p)_f}\},$$

$$\varphi_7=(1-\varphi)$$

$$f'(\eta)=u(\eta) \qquad (15)$$

$$u'(\eta)=v(\eta) \qquad (16)$$

$$v'(\eta)=-\varphi_1\left(\frac{a^2}{c^2}-\left(f'\right)^2+f\ f''\right)-\left(\lambda+M\varphi_5\right)\left(\frac{a}{c}-f'\right)-\varphi_4\gamma_1\left(\theta+\gamma\ \varphi\right) \qquad (17)$$

$$\theta'(\eta)=p(\eta) \qquad (18)$$

$$p'(\eta)=-\frac{\Pr}{\left(\frac{K_{nf}}{K_f}+N_r\right)}\left(\delta\theta+\frac{Ec}{\varphi_5}\left(f''\right)^2+\varphi_6 f\theta'-2\varphi_6 f'\theta\right) \qquad (19)$$

$$\varphi'(\eta) = Q(\eta) \tag{20}$$

$$q'(\eta) = -\frac{Sc}{\varphi_7}\left(f\varphi' - 2f'\varphi - \gamma_2\varphi\right) \tag{21}$$

IC:

$$f(0) = S, u(0) = \pm 1, v(0) = \alpha, \theta(0) = 1, p(0) = \beta, \varphi(0) = 1, q(0) = \tau \tag{22}$$

BC: $$f'(\infty) = \frac{a}{c}, \theta(\infty) = 0, \varphi(\infty) = 0 \tag{23}$$

α, β and τ are the unknowns to be obtained as a part of the solution. By using DSolve subroutine command in MAPLE 18, we can get the solution for the equations (15)-(23) with trial and error basis. This software consists of fourth-fifth order Runge–Kutta–Fehlberg method with shooting technique and the Maple worksheet is illustrated in Appendix A. The numerical results are obtained the velocity, temperature, concentration, skin friction, rate of heat and mass transfer in the presence of Cu –water and SWCNT –water.

III. RESULTS AND DISCUSSION

Equations (9) - (11) with boundary conditions (13) have been solved numerically using fourth-fifth order Runge–Kutta–Fehlberg method with shooting technique (MAPLE 18) with the fixed values of the parameters: $\Pr = 6.8, Sc = 1.0, M = 1.0,$ $\lambda = 0.2, \delta = 0.5, \gamma = 0.5, \gamma_1 = 1.0, \gamma_2 = 0.8, Ec = 0.1$ *and* $Nr = 1.0$. Validate our technique, $-f''(0)$ as compared with those of Kameswaran et al. [16] and found them in good agreement, see Table 2.

Table 1: Thermophysical properties of fluid and nanoparticles

	$\rho (kg/m^3)$	$c_p (J/kgK)$	$k (W/mK)$	$\beta_T \times 10^{-5} (K^{-1})$	$\beta_C \times 10^{-5} (K^{-1})$	$\alpha \times 10^{-7} (m^2/s)$
Pure water	997.1	4179	0.613	21	63	1.47
Seawater	1021	4000	0.6015	4.181	12.543	1.46
Copper (Cu)	8933	385	401	1.67	5.01	1163.1
Alumina (Al_2O_3)	3970	765	40	0.85	2.55	131.7
Titanium (TiO_2)	4250	6862	8.9538	0.9	2.7	30.7
SWCNTs	2600	425	6600	0.33	0.99	2.0

Table 2: Comparison of $-f''(0)$ for different values of φ with $Sc = 1.0, \Pr = 6.2, \lambda = 0.2, \gamma = 0, \gamma 1 = 0, \gamma 2 = 0.1, Ec = 0.1, M = 0.0$

φ	Kameswaran et al.[16] $-f''(0)$	Present result $-f''(0)$	Absolute error
0.05	1.108919904	1.10893772367974	0.000012
0.1	1.174746021	1.17477541087648	0.000026
0.15	1.208862320	1.20889945528981	0.000030
0.2	1.218043809	1.2180860392435	0.000042

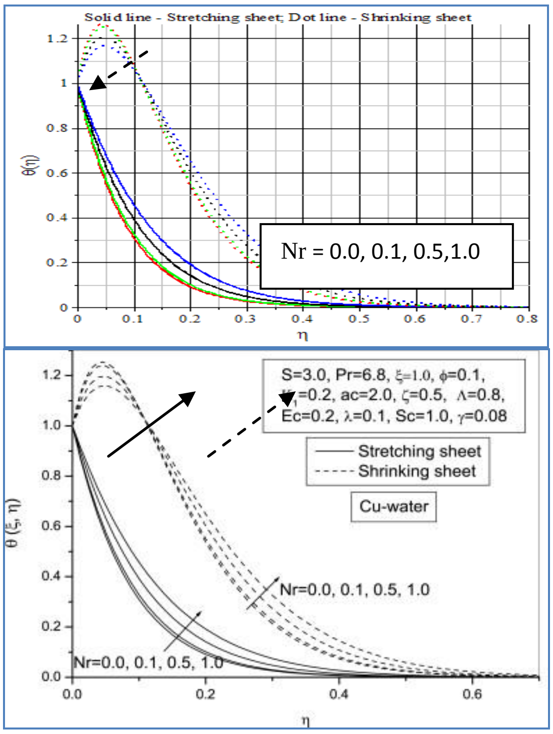

Fig. 2: Comparison of temperature profile for Nr with Fig. 3 of Dulal and Gopinath Mandal [15]

The temperature profiles for different values of Nr Fig. 2 is significantly correlated with Fig.3 of Dulal Pal Gopinath Mandal [15].

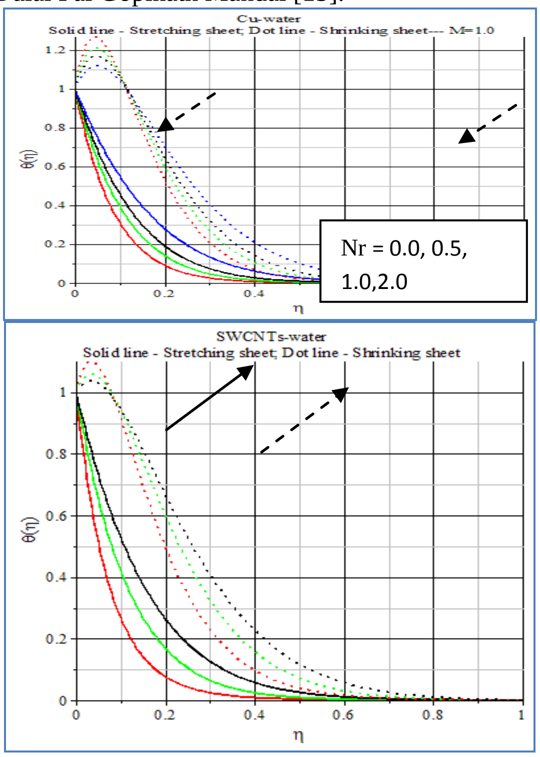

Fig. 3: Thermal radiation effects on temperature profiles

Table 3a: $f''(0)$, $-\theta'(0)$ and $-\phi'(0)$ for different values of Nr in Cu-water with $Sc = 1.0, Pr = 6.8, \lambda = 0.2, \gamma = 0.5, \gamma_1 = 1.0, \gamma_2 = 0.5, Ec = 0.2, \delta = 0.1, \frac{a}{c} = 2.0$

Surface	Nr	$f''(0)$	$-\theta'(0)$	$-\phi'(0)$
Stretching	0.0	5.600290501583693	11.41958541204386	4.50042559857023
	0.5	5.586438399107651	8.845091417966374	4.42347223884488
	1.0	5.59466312881225	7.290474719620383	4.42370774468370
	2.0	5.608966206151345	5.503802659060943	4.42416126249365
Shrinking	0.0	15.36806424513948	-14.07351289884172	3.83041307891423
	0.5	15.37442898721037	-10.30185749140587	3.83078196783442
	1.0	15.38009078991273	-8.047774247037397	3.83111298757976
	2.0	15.38975024009687	-5.4844593[illegible]	3.8316810[illegible]

Table 3b: $f''(0)$, $-\theta'(0)$ and $-\phi'(0)$ for different values of Nr in SWCNTs-water with $Sc = 1.0, Pr = 6.8, \lambda = 0.2, \gamma = 0.5, \gamma 1 = 1.0, \gamma 2 = 0.5, Ec = 0.2, \frac{a}{c} = 2.0, M = 1.0$

Surface	Nr	$f''(0)$	$-\theta'(0)$	$-\phi'(0)$

Stretching	0.5	4.293115056090663	13.5045061866853	4.37236249108178
	1.0	4.286690517790732	8.43380893813833	4.37234748079110
	2.0	4.304381035228571	6.10911944052156	4.37292278717011
Shrinking	0.5	11.61047302421111	-6.62434840449701	3.73875855331480
	1.0	11.62603988686511	-3.67610506756365	3.73959395660315
	2.0	11.63973639237166	-2.31592360208240	3.74036744049350

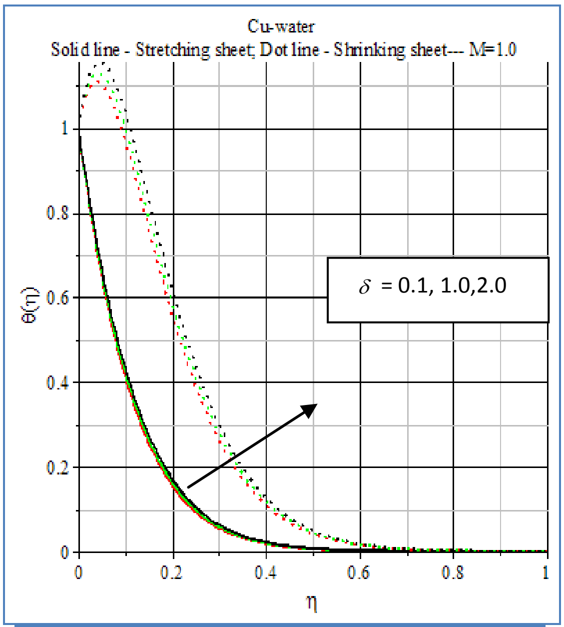

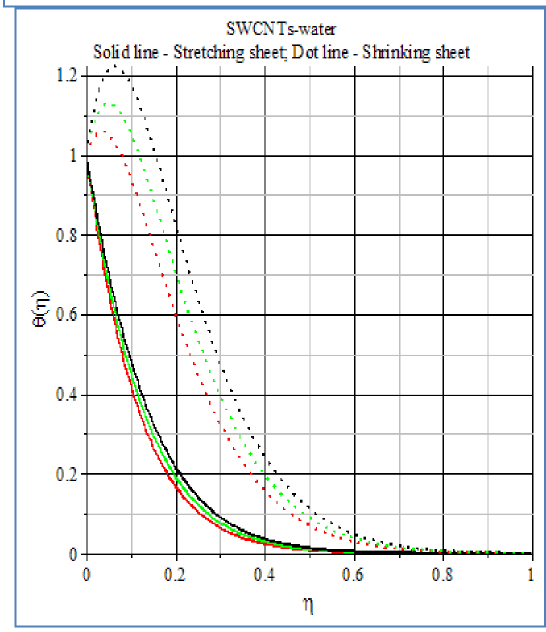

(a)

(b)

Fig. 4: Heat source effects on temperature profiles

Table 4a: $f''(0)$, $-\theta'(0)$ and $-\phi'(0)$ for different values of δ in Cu-water with $Sc = 1.0, \Pr = 6.8, \lambda = 0.2, \gamma = 0.5, \gamma 1 = 1.0, \gamma 2 = 0.5, Ec = 0.2, M = 3.0, \frac{a}{c} = 2.0$

Surface	δ	$f''(0)$	$-\theta'(0)$	$-\phi'(0)$

Stretching	0.1	5.43904085412932	8.461037107206627	4.31348122330852
	1.0	5.41081561232620	8.198962024649298	4.23781328505081
	2.0	5.41240262367156	7.884937127014190	4.23785741441042
Shrinking	0.1	14.9577638424221	-6.315515022532462	3.65938229746317
	1.0	14.9629315582706	-6.975114914919485	3.65956476310953
	2.0	14.9693053347662	-7.767065757635182	3.65979123045349

Table 4b: $f''(0)$, $-\theta'(0)$ and $-\phi'(0)$ for different values of δ in SWCNTs-water with $Sc = 1.0, \Pr = 6.8, \lambda = 0.2, \gamma = 0.5, \gamma 1 = 1.0, \gamma 2 = 0.5, Ec = 0.2,$

Surface	δ	$f''(0)$	$-\theta'(0)$	$-\phi'(0)$
Stretching	0.1	4.317177355312274	8.42660389152805	4.37301816974440
	1.0	4.291254568268895	7.61125477853972	4.37248413030351
	2.0	4.295847549094079	6.85593263143991	4.37262463488123
Shrinking	0.1	11.62603988686586	-3.67610506756162	3.73959395660353
	1.0	11.64686974592099	-5.87158986679762	3.74042630852011
	2.0	11.67014030251707	-8.15756112592031	3.74136864476395

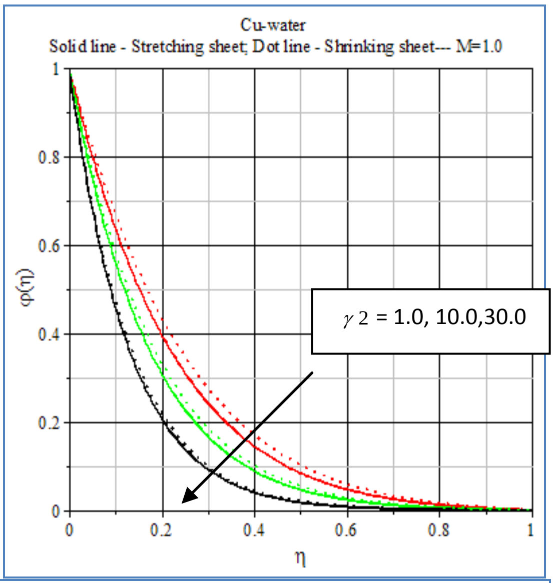

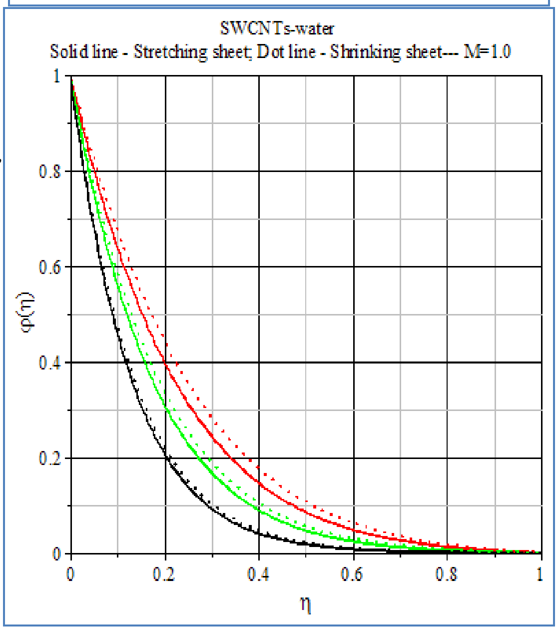

(a)

(b)

Fig. 5: Chemical reaction effects on concentration profiles

Table 5a: $f''(0)$, $-\theta'(0)$ and $-\phi'(0)$ for different values of $\gamma 2$ in Cu-water with $Sc = 1.0, \Pr = 6.8, \lambda = 0.2, \gamma = 0.5, \gamma 1 = 1.0, \delta = 0.5, Ec = 0.2, M = 1.0,$

Surface	$\gamma 2$	$f''(0)$	$-\theta'(0)$	$-\phi'(0)$
Stretching	1.0	5.43904085412932	8.461037107206627	4.31348122330852
	10.0	5.41081561232620	8.198962024649298	4.23781328505081
	30.0	5.41240262367156	7.884937127014190	4.23785741441042
Shrinking	1.0	14.9577638424221	-6.315515022532462	3.65938229746317
	10.0	14.9629315582706	-6.975114914919485	3.65956476310953
	30.0	14.9693053347662	-7.767065757635182	3.65979123045349

Table 5b: $f''(0)$, $-\theta'(0)$ and $-\phi'(0)$ for different values of $\gamma 2$ in SWCNTs-water with

$Sc = 1.0, \Pr = 6.8, \lambda = 0.2, \gamma = 0.5, \gamma 1 = 1.0, \gamma 2 = 0.5, Ec = 0.2, M$

Surface	$\gamma 2$	$f''(0)$	$-\theta'(0)$	$-\phi'(0)$
Stretching	1.0	4.60417086470682	8.34321536422733	4.38034162861773
	10.0	4.566262100446633	8.35426607662824	5.68810180585984
	30.0	4.557059850139283	8.35802232490946	7.71070046850420
Shrinking	1.0	12.59895851011825	-4.52876073732553	3.77049704561112
	10.0	12.58787173525841	-4.51385064746607	5.22092200379669
	30.0	12.57660230258925	-4.50001983004193	7.36823364276058

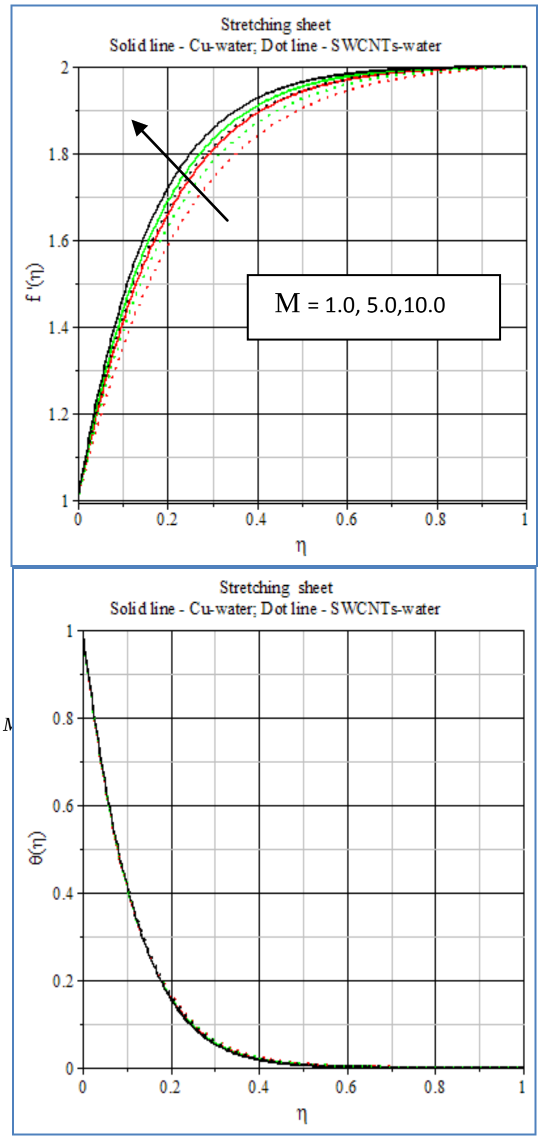

Fig. 6: Magnetic strength on velocity and temperature profiles

Table 6: $f''(0)$ and $-\theta'(0)$ for different values of M with

$Sc = 1.0, \Pr = 6.8, \lambda = 0.2, \gamma = 0.5, \gamma 1 = 1.0, \gamma 2 = 0.5, Ec = 0.2, \frac{a}{c} = 2.0,$

Stretching	M	$f''(0)$	$-\theta'(0)$
Cu-water	1.0	5.188464775294874	8.4174804149269
	5.0	5.646047061412568	8.2794486106085
	10.0	6.183713754659339	8.1153794515745
SWCNTs-water	1.0	4.287407045707617	8.43349550693229
	5.0	4.841069375502433	8.27194954995582
	10.0	5.432411723521107	8.09416015553817

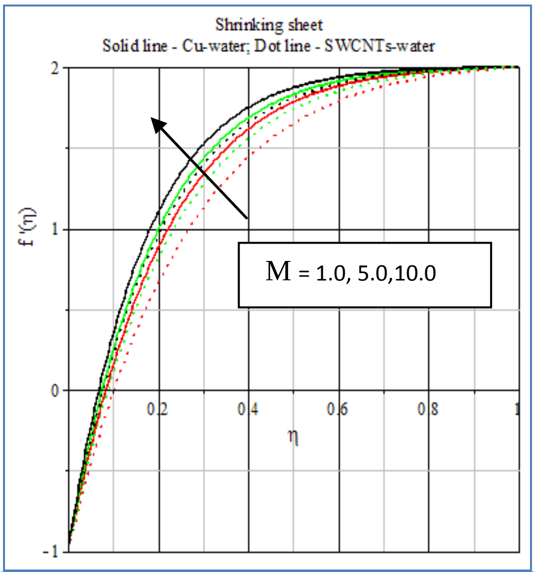

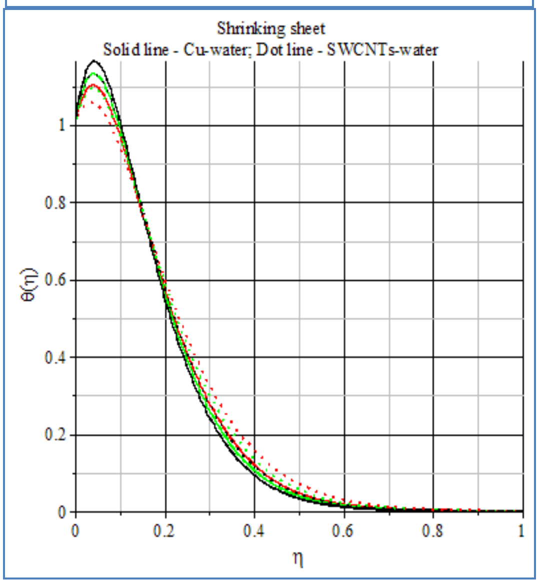

Fig. 7: Magnetic strength on velocity and temperature profiles

Table 7: $f''(0)$ and $-\theta'(0)$ for different values of M with $Sc = 1.0, \Pr = 6.8, \lambda = 0.2, \gamma = 0.5, \gamma 1 = 1.0, \gamma 2 = 0.5, Ec = 0.2, \frac{a}{c} = 2.0, N = 1.0$

Shrinking	M	$f''(0)$	$-\theta'(0)$
Cu-water	1.0	14.16136731518859	-5.8772164983436
	5.0	15.74640397763432	-7.3254313150657
	10.0	17.50494614036955	-8.9705041495712
SWCNTs-water	1.0	1.626039886865860	-3.6761050675616
	5.0	13.48049956014150	-5.32072176479851
	[illegible]	[illegible]2369495402	-7[illegible]

M = 1.0, 5.0,10.0

In the presence of stretching sheet, the temperature of Cu– water and SWCNTs-water increases, whereas it firstly decreases and then increases for shrinking sheet with increase of thermal radiation, Figs. 3a and 3b. The thermal boundary layer thickness for SWCNTs-water is stronger than that of Cu-water. The rate of heat transfer for water based Cu and SWCNTs decreases for stretching sheet, but it increases for shrinking sheet with increase of thermal radiation. In the presence of shrinking sheet, the rate of heat transfer for SWCNTs - water is stronger compared as Cu-water because of the thermal conductivity of SWCNTs $(k = 6600)$ and Copper $(k = 401)$, Tables 3a and 3b. Both stretching and shrinking sheets, the temperature of the nanofluids (Cu-water and SWCNTs-water) increases with the increase of heat source, whereas the thermal boundary layer thickness for SWCNTs-water is stronger than that of Cu-water because of the density of SWCNTs $(\rho = 2600)$ and Copper $(\rho = 8933)$, Figs. 4a and 4b. The heat transfer rate decreases with the increase of heat source and there is no significant difference in skin friction coefficient and rate of mass transfer with the increase of heat source, Tables 4a and 4b. Both stretching and shrinking sheets, the concentration of the Cu-water and SWCNTs-water decreases with increase of chemical reaction, Figs. 5a and 5b. The rate of mass transfer of SWCNTs-water is more energetic than that of Cu-water to increase of chemical reaction (Tables 5a and 5b) because of the kinematic viscosity of the nanofluids. In the presence of stretching and shrinking sheets, the velocity of the water based copper and SWCNTs increases with increase of magnetic strength. The temperature of the nanofluids (Cu-water and SWCNTs-water) firstly increases and then decreases for shrinking sheet and there is no significance difference in stretching sheet with increase of magnetic strength, Figs. 6 and 7. Both stretching and shrinking sheet, the skin friction increases and the rate of heat transfer of water based Cu and SWCNTs decreases with increase of magnetic strength, Tables 6 and 7. The thermal boundary layer thickness for Cu-water is firstly stronger than that of SWCNTs-water and then SWCNTs-water is more forceful than that of Cu-water to increase of magnetic strength because of the Lorentz force acts in the opposite direction to the flow field and tends to raise its temperature.

IV. CONCLUSION

In the present investigation, the following conclusion is drawn:

In the presence of shrinking sheet An important result is the broad exaggeration of the temperature field caused for the increasing of thermal radiation, magnetic strength and heat source since there is a peak formation of temperature distribution is predicted in the outer boundary region.The thermal boundary layer thickness for SWCNTs-water is stronger as compared to Cu-water with increase of thermal radiation and heat source.

In the presence of stretching sheet The temperature of water based copper and SWCNTs increases with increase of thermal radiation and heat source, whereas the rate of heat transfer for SWCNTs-water is more significant compared to Cu-water with increase of thermal radiation and heat source. Both stretching and shrinking sheets

(i) The diffusion boundary layer thickness for SWCNTs-water is more capable compared to that of Cu-water to increase of chemical reaction.

(ii) The momentum and thermal boundary layer thickness for SWCNTs-water is more active compared to Cu-water with increase of magnetic strength.

SWCNTs-water due to thermal radiation energy in the presence of magnetic field along the shrinking sheet plays a dominant role on heat and mass transfer because they can be used in numerous applications such as solar collectors, drying processes, heat exchangers, geothermal and oil recovery, building construction, etc. The integrative investigation on water based SWCNTs presents a great opportunity for exploration and discovery at the frontiers of nanotechnology.

Nomenclature

B_0 Magnetic flux density, $kg\ s^{-2} A^{-1}$

C Concentration of the fluid, K

C_w Concentration of the wall, K

C_∞ Concentration of the fluid far away from the wall, K

c_p Specific heat at constant pressure, $J\ kg^{-1} K^{-1}$

Dm Specific Diffusivity, $m^2\ s^{-1}$

Ec Eckert number, $\dfrac{u_w^2}{\Delta T (c_p)_f}$, $\dfrac{(m\ s^{-1})^2 s^2 K}{K\ m^2}$ (-)

g Acceleration due to gravity, ms^{-2}

k_1 First order rate of chemical reaction, s^{-1}

k^* mean absorption coefficient, m^{-1}

K Permeability of the porous medium, m^2

k_f Thermal conductivity of the base fluid, $kg\ m\ s^{-3}\ K^{-1}$

k_s Thermal conductivity of the nanoparticle, $kg\ m\ s^{-3}\ K^{-1}$

k_{nf} Effective thermal conductivity of the nanofluid, $kg\ m\ s^{-3}\ K^{-1}$

M Magnetic parameter, $\dfrac{\sigma B_0^2 x}{u_w \rho_f}, \left(\dfrac{\Omega^{-1} m^{-1} B_0^2\ m}{m\ s^{-1}\ kg\ m^{-3}}\right)$ (-)

N Thermal radiation parameter, $\dfrac{16 \sigma_1 \theta_w^3}{3 k_f\ k^*} = \left(\dfrac{kg\ s^{-3} K^{-4} K^3}{kg\ m\ s^{-3} K^{-1} m^{-1}}\right)$ (-)

Pr Prandtl number, $\dfrac{\nu_f}{\alpha_f} = \left(\dfrac{m^2 s^{-1}}{m^2 s^{-1}}\right)$ (-)

q''_{rad} Incident radiation flux of intensity, $kg\ m^{-1}\ s^{-3}\ K^{-1}$

Q_0 Rate of source/sink, $kg\ m^{-2}$

Sc Schmidt number, $\frac{\nu_f}{D_f}, \frac{m^2\ s^{-1}}{m^2\ s^{-1}}$ (-)

T Temperature of the fluid, K

T_w Temperature of the wall, K

T_∞ Temperature of the fluid far away from the wall, K

x, y Streamwise coordinate and cross-stream coordinate, m

u, v Velocity components in x and y direction, $m\ s^{-1}$

$U(x)$ Flow velocity of the fluid away from the wedge, $m\ s^{-1}$

V_0 Velocity of suction / injection, $m\ s^{-1}$

Greek symbols

α_{nf} Thermal diffusivity of the nanofluid, $m^2\ s^{-1}$

β_f Thermal expansion coefficients of the base fluid, K^{-1}

ρ_f Density of the base fluid, $kg\ m^{-3}$

ρ_s Density of the nanoparticle, $kg\ m^{-3}$

ρ_{nf} Effective density of the nanofluid, $kg\ m^{-3}$

$(\rho\ c_p)_{nf}$ Heat capacitance of the nanofluid, $J\ m^{-3} K^{-1}$

$(\rho\ \beta)_{nf}$ Volumetric coefficient of thermal expansion of nanofluid, K^{-1}

σ Electrical conductivity, $\Omega^{-1} m^{-1}$

σ_1 Stefan – Boltzmann constant, $kg\ s^{-3}\ K^{-4}$

μ_f Dynamic viscosity of the base fluid, $kg\ m^{-1}\ s^{-1}$

μ_{nf} Effective dynamic viscosity of the nanofluid, $kg\ m^{-1}\ s^{-1}$

γ Buoyancy ratio, $\frac{(\beta_C)_f\ \Delta C}{(\beta_T)_f\ \Delta T}\left(\frac{K^{-1}K}{K^{-1}K}\right)$ (-)

$\gamma 1$ Mixed convection parameter, $\frac{(\beta_T)_f\ g \Delta Tx}{u_w^2}\left(\frac{K^{-1} m\ s^{-2} K\ m}{(m\ s^{-1})^2}\right)$ (-)

$\gamma 2$ Chemical reaction parameter, $\frac{k_1 x}{u_w}\left(\frac{s^{-1} m}{m\ s^{-1}}\right)$ (-)

ν_{nf} Dynamic viscosity of the nanofluid, $m^2\ s^{-1}$

δ Heat source / sink parameter, $\frac{Q_0\ x}{(\rho\ c_p)_f\ u_w}, \left(\frac{kg\ m^{-1} s^{-3} K^{-1} m}{kg\ m^{-2} s^{-1} (m^2\ s^{-2} K^{-1})}\right)$ (-)

λ Porous parameter, $\frac{\nu_f\ x}{K\ u_w}\left(\frac{m^2 s^{-1}\ m}{m\ m^2 s^{-1}}\right)$ (-)

Ω Resistance, $kg\ m^2 s^{-3} A^{-2}$

ξ Distance along the wedge, (m)

ζ Nanoparticle volume fraction, (-)

ψ Dimensionless stream function, (-)

η Similarity variable, (-)

f Dimensionless stream function, (-)

θ, φ Dimensionless stream function, (-)

REFERENCES

[1]. Choi et al., 2001, S.U.S. Choi, Z.G. Zhang, W. Yu, F.E. Lockwood, E.A. Grulke, Anomalously thermal conductivity enhancement in nano tube suspensions, Appl. Phys. Lett., 79 (2001), pp. 2252–2254.

[2]. J. Buongiorno, L. Hu, Innovative technologies: two-phase heat transfer in water-based nanofluids for nuclear applications, final report, Tech. report, Massachusetts Institute of Technology (2009).

[3]. S.J. Kim, T. McKrell, J. Buongiorno, L.-W. Hu, Experimental study of flow critical heat flux in alumina– water, zinc–oxide–water, and diamond–water nanofluids, J. Heat Transfer, 131 (4) (2009), p. 043204.

[4]. D. Zhu, S. Wu, N. Wang, Thermal physics and critical heat flux characteristics of Al_2O_3–H_2O nanofluids Heat Transfer Eng., 31 (14) (2010), pp. 1213–1219.

[5]. J. Buongiorno, L.W. Hu, Nanofluid heat transfer enhancement for nuclear reactor applications

[6]. J. Energy Power Eng., 4 (6 (Serial No. 31)) (2010), pp. 1–8.

[7]. R.S.R. Gorla, A.J. Chamkha, A.M. Rashad, Mixed convective boundary layer flow over a vertical wedge embedded in a porous medium saturated with a nanofluid: natural convection dominated regime, Nanoscale Res. Lett., 6 (2011), p. 207 http://dx.doi.org/10.1186/1556-276X-6-207.

[8]. M.J. Uddin, W.A. Khan, A.I.M. Ismail, Free convection boundary layer flow from a heated upward facing horizontal flat plate embedded in a porous medium filled by a nanofluid with convective boundary

condition, , Transp. Porous Med., 93 (2012), pp. 867–881.

[9]. M.A.A. Hamad, M. Ferdows, Similarity solution of boundary layer stagnation-point flow towards a heated porous stretching sheet saturated with a nanofluid with heat absorption/generation and suction/blowing: a Lie group analysis, Commum. Nonlinear Sci. Numer. Simulat., 17 (1) (2011), pp. 132–140.

[10]. P. Rana, R. Bhargava, Flow and heat transfer of a nanofluid over a nonlinearly stretching sheet: a numerical study, Commun. Nonlinear Sci. Numer. Simulat., 17 (2012), pp. 212–226.

[11]. 10. N.C. Rosca, T. Grosan, I. Pop, Stagnation-point flow and mass transfer with chemical reaction past a permeable stretching/shrinking sheet in a nanofluid, Sains Malaysiana, 41 (10) (2012), pp. 1271–1279.

[12]. V. Rabikumar, M.C. Raju, G.S.S. Raju, Heat and mass transfer effects on MHD flow of viscous fluid through non-homogeneous porous medium in the porous medium in presences of temperature dependent heat source, Int. J. Contemp. Math. Sci., 7 (32) (2012), pp. 1597–1604.

[13]. M.M. Rahman, M.A. Al-Lawatia, I.A. Eltayeb, N. Al-Salti, Hydromagnetic slip flow of water based nanofluids past a wedge with convective surface in the presence of heat generation (or) absorption, Int. J. Thermal Sci., 57 (2012), pp. 172–182.

[14]. R. Kandasamy, P. Loganathan, P. Puvi Arasu, Scaling group transformation for MHD boundary-layer flow of a nanofluid past a vertical stretching surface in the presence of suction/injection, Nucl. Eng. Design, 241 (6) (2011), pp. 2053–2059.

[15]. S.M. AbdEl-Gaied, M.A.A. Hamad, MHD forced convection laminar boundary layer flow of alumina–water nanofluid over a moving permeable flat plate with convective surface boundary condition, J. Appl. Math. (2013) Article ID 403210, 8 p.

[16]. Dulal Pal and Gopinath Mandal, Influence of thermal radiation on mixed convection heat and mass transfer stagnation-point flow in nanofluids over stretching / shrinking sheet in a porous medium with chemical reaction, Nuclear Engineering and Design, 273(2014), pp. 644-652.

[17]. P.K. Kameswaran, M. Narayana, P. Sibanda, P.V.S.N. Murthy, Hydromagnetic nanofluid flow due to a stretching or shrinking sheet with viscous dissipation and chemiical reaction effects, Int. J. Heat Mass Transfer, 55 (25-26) (2012), pp. 7587–7595

Appendix A

$> restart;$

$> libname := Shootlib, libname:$

$> with(Shoot):$

$> Pr := 6.2; s := 0.2; \Upsilon := 0.05; \lambda := 0.2; G := 0.5; G1 := 1; G2 := 0.08; Ec := 0.1; Sc := 1.0;$

$Pr := 6.2, s := 0.2, \Upsilon := 0.05, \lambda := 0.2, G := 0.5, G1 := 1, G2 := 0.08, Ec := 0.1, Sc := 1.0$

$> M := 0; Z := 0.1; \Xi := 0.5; N := 1; \delta := 0.5;$

$M := 0, Z := 0.1, N := 1, \delta := 0.5$

$>$

$(CT) := 0.5; (\rho s) := 8933; (\rho f) := 997; (cps) := 385; (cpf) := 4179; (ks) := 401; (kf) := 0.613; (\beta Ts) := 1.67\mathrm{E}{-5}; (\beta Tf) := 21\mathrm{E}{-5};$

$CT := 0.5, \rho s := 8933, \rho f := 997, cps := 385, cpf := 4179, ks := 401, kf := 0.613, \beta Ts := 0.0000167, \beta Tf := 0.00021$

$> (Kfn) := (ks) + 2.(kf) - 2.\Upsilon.((kf) - (ks));$

$Kfn := 442.26470$

$> a := (1-\Upsilon)^{2.5}.\left(1 - \Upsilon + \Upsilon.\frac{(\rho s)}{(\rho f)}\right);$

$a := 1.229742875$

$> l := \left(1 - \Upsilon + \Upsilon.\frac{(\rho s).(cps)}{(\rho f).(cpf)}\right);$

$l := 0.9912724774$

$> d := (1-\Upsilon)^{2.5}.\left(1 - \Upsilon + \Upsilon.\frac{(\rho s).(\beta Ts)}{(\rho f).(\beta Tf)}\right);$

$d := 0.8670042920$

$> b := \left(1 - \Upsilon + \Upsilon.\frac{(\rho s).(\beta Ts)}{(\rho f).(\beta Tf)}\right);$

$b := 0.9856261881$

$> c := \left(1 - \Upsilon + \Upsilon.\frac{(\rho s).(\beta Cs)}{(\rho f).(\beta Cf)}\right);$

$c := 0.95 + \frac{0.4479939819\, \beta Cs}{\beta Cf}$

$>$

$> e := (1-\Upsilon)^{2.5};$

$e := 0.8796481896$

$> (Kf) := (ks) + 2.(kf) + 2.\Upsilon.((kf) - (ks));$

$Kf := 362.18730$

$> p := \frac{Kfn}{Kf};$

$p := 1.221093893$

> $q := (1 - \Upsilon);$

$q := 0.95$

>

> $FNS := \{f(\eta), u(\eta), v(\eta), \theta(\eta), r(\eta), \varphi(\eta), h(\eta)\}:$

>

>

$$ODE := \Big\{\mathrm{diff}(f(\eta),\eta) = u(\eta), \mathrm{diff}(u(\eta),\eta) = v(\eta), \mathrm{diff}(\theta(\eta),\eta) = r(\eta), \mathrm{diff}(\varphi(\eta),\eta) = h(\eta), \mathit{diff}(v(\eta),\eta) + a.\left(-u(\eta)^2 + f(\eta).v(\eta)\right) - M.e.u(\eta) = 0, \mathrm{diff}(r(\eta),\eta) + \frac{Pr}{p}.J.\left(\frac{Ec}{e}.v(\eta)^2 + f(\eta).r(\eta) - (2.0).u(\eta).\theta(\eta)\right) = 0, \mathit{diff}(h(\eta),\eta) + Sc.\left(f(\eta).h(\eta) - (2.0).u(\eta).\varphi(\eta) - G2.\varphi(\eta)\right) - s.\frac{Pr}{p}.J.\left(\frac{Ec}{e}.v(\eta)^2 + f(\eta).r(\eta) - (2.0).u(\eta).\theta(\eta)\right) = 0\Big\};$$

$$ODE := \Big\{\frac{d}{d\eta}v(\eta) - 1.229742875\,u(\eta)^2 + 1.229742875\,(f(\eta).v(\eta)) = 0, \frac{d}{d\eta}r(\eta) + 0.5721720846\,v(\eta)^2 + 5.033101382\,(f(\eta).r(\eta)) - 10.06620276\,(u(\eta).\theta(\eta)) = 0, \frac{d}{d\eta}h(\eta) + 1.0\,(f(\eta).h(\eta)) - 2.00\,(u(\eta).\varphi(\eta)) - 0.080\,\varphi(\eta) - 0.1144344170\,v(\eta)^2 - 1.006620277\,(f(\eta).r(\eta)) + 2.013240554\,(u(\eta).\theta(\eta)) = 0, \frac{d}{d\eta}f(\eta) = u(\eta), \frac{d}{d\eta}\theta(\eta) = r(\eta), \frac{d}{d\eta}u(\eta) = v(\eta), \frac{d}{d\eta}\varphi(\eta) = h(\eta)\Big\}$$

> $IC := \{f(0) = 0, u(0) = 1, \theta(0) = 1, \varphi(0) = 1, v(0) = \alpha, r(0) = \tau, h(0) = \varsigma\};$

$IC := \{f(0) = 0, h(0) = \varsigma, r(0) = \tau, \theta(0) = 1, u(0) = 1, v(0) = \alpha, \varphi(0) = 1\}$

> $L := 100;$

$L := 100$

> $BC := \{u(\mathrm{L}) = 0, \theta(\mathrm{L}) = 0, \varphi(L) = 0\};$

$BC := \{\theta(100) = 0, u(100) = 0, \varphi(100) = 0\}$

> $infolevel[shoot] := 1:$

> $S := shoot(ODE, IC, BC, FNS, [\alpha = -1.108937723679742, \tau = -3.1519633343887605, \varsigma = -0.8747609797555731]):$

shoot: Step # 1
shoot: Parameter values : alpha = -1.108937723679742 tau = -3.1519633343887605 ς = -.8747609797555731